Routes to Alkene and Epoxide Functionalized Nanoporous Materials from Poly(styrene-*b*-isoprene-*b*-lactide) Triblock Copolymers

Travis S. Bailey, Javid Rzayev, and Marc A. Hillmyer*

Department of Chemistry, University of Minnesota, Minneapolis, Minnesota 55455

Received August 16, 2006; Revised Manuscript Received September 26, 2006

ABSTRACT: Nanoporous materials with inherently tunable surface chemistries are poised to have a considerable impact in catalysis, separations, and nanopatterning. Using core−shell cylinder forming polystyrene-*b*-polyisoprene-*b*-polylactide (PS−PI−PLA) triblock terpolymers as templates, we were able to prepare aligned PI-coated nanoporous PS monoliths via the degradative removal of the cylindrical PLA cores. PS−PI−PLA precursors were synthesized using a combination of anionic (PS, PI) and ring-opening (PLA) polymerizations. The degree of order, alignment, and PLA degradation achievable was a strong function of molecular weight at a given triblock terpolymer composition. For intermediate molecular weight samples (25−28 kg mol^{-1}), greater than 95% of the PLA was hydrolyzed through exposure of the monolith to a 0.1 wt % sodium dodecyl sulfate (SDS) solution in 0.5 N NaOH. However, low (17.5 kg mol^{-1}) and high (46.8 kg mol^{-1}) molecular weight samples of identical composition showed considerable resistance to PLA degradation. Treatment of the degraded monoliths with *m*-chloroperoxybenzoic acid in aqueous *tert*-butyl alcohol solutions permitted the controlled epoxidation of up to 75−80% of the PI alkene units. Despite some loss in pore alignment, scanning electron microscopy and small-angle X-ray scattering verified the retainment of the nanoporous structure following epoxidation.

Introduction

As a result of their inherently high internal surface areas and uniform pore dimensions at the nanometer length scale, the synthesis of nanoporous materials by a variety of techniques has received great attention. A number of the fabrication strategies have exploited the controlled and periodic domain structures generated in self-assembled block copolymer melts and solutions.[1−9] Inorganic materials, such as those based on silicon, aluminum, and titanium oxides, are typically generated using solution-templated condensation processes that produce rigid scaffolds offering excellent thermal and chemical stability. Polymeric nanoporous matrices, in contrast, are typically generated through the selective chemical, UV, or thermal etching of one or more minority component domains from a macroscopically ordered and aligned block copolymer precursor.[1] Unlike the brittle inorganic oxides, the mechanical character of polymeric matricies can be tuned, in theory, from elastic[10] to rigid[11] by virtue of the numerous possible permutations of block copolymer precursors available. As a result, such nanoporous materials have been promoted for their potential versatility as both sacrificial templates and working substrates in a host of applications, including those involving patterning resists,[12−15] catalyst supports, and controlled separations media.

In previous work, we have been able to generate a collection of polymer-based nanoporous materials exploiting the selective chemical degradation of minority component domains from various AB diblock and ABC triblock precursors. Our recent efforts have focused on synthetic routes for the insertion of specific chemical functional groups within the pore interior of these materials, as being able to specifically define the analyte−surface interactions within the pore space itself is critical to many of the above applications.[16−18] The challenges faced, in this regard, are often of two general forms: (1) ensuring the compatibility between the functional group to be inserted and the processing or etch steps used to generate the nanoporous structure or (2) ensuring the compatibility between the reaction conditions used to insert or transform a functional group and the integrity of the nanoporous framework in that environment.

Using post-etch transformations, creative blending strategies, and calculated block selections, we have had recent success integrating a range of functional groups into AB diblock and ABC triblock derived nanoporous substrates. The generation of porosity from these precursors has been generally based on the selective chemical removal of polylactide (PLA) or poly(ethylene oxide) (PEO) domains from the self-assembled cylinder and gyroid microphases of these materials.[9−11,16−20] Interestingly, both of these etch processes have the inherent benefit of generating residual hydroxyl functional groups at the pore wall. However, in both polystyrene (PS)[19,20] and polycyclohexylethylene (PCHE)[11] substrates, the areal density of these groups was found insufficient to alter the hydrophobicity of the pore interior to an extent permitting the penetration of aqueous media.

To overcome this limitation, we have developed several strategies aimed at improving the hydrophilicity of the interior pore space. Using a PS−PEO/PS−PLA diblock copolymer blending strategy, Mao et al.[16] were able to generate nanoporous PS monoliths with PEO coated pores exhibiting a universal tendency to imbibe water, in contrast to identical samples generated without the blended PS−PEO diblock copolymer. More recently, Rzayev et al.[17] achieved a similar pore hydrophilicity exploiting core−shell cylinder forming poly(styrene-*b*-dimethylacrylamide-*b*-lactide) (PS−PDMA−PLA) triblock copolymer precursors, in which the water-soluble PDMA midblock is left at the pore surface after selective removal of the sacrificial PLA core. Notably, in both the blending and core−shell strategies outlined above, the opportunity to control the functional group density of the hydrophilic repeat unit is possible simply by varying the composition of the blend (in the strategy of Mao et al.) or, alternatively, the molecular weight of the hydrophilic block (applicable to both methods).

* Corresponding author: e-mail hillmyer@chem.umn.edu.

10.1021/ma061892b CCC: $33.50
Published on Web 11/15/2006

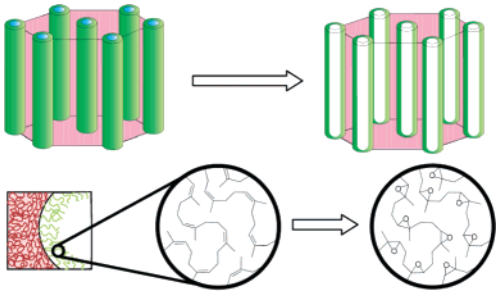

Figure 1. Generalized strategy for the formation of functionalized nanoporous materials from the core−shell cylinder morphology of an ABC triblock copolymer, in which the exposed shell block is chosen for its susceptibility to future modification. In this work, we demonstrate the utility of this strategy to introduce epoxide groups at the pore surface via direct oxidation of an exposed polyisoprene shell circumscribing each pore.

Perhaps more importantly, the true versatility of Rzayev et al.'s original ABC approach was demonstrated in a subsequent publication,[18] in which they were able to exploit the inherent functionality of the exposed B-block to further tailor the surface chemistry of the pore. Through acidic hydrolysis they were able to easily transform the amide pendant groups in the PDMA chains to their corresponding acid, effectively introducing water-soluble and pH-responsive poly(acrylic acid) (PAA) into the pores. Subsequent modification of the pore interior through acid−amine coupling reactions were then used to introduce a variety of additional functional groups, including pyridine, a terminal alkene, and a chiral alcohol, in a further demonstration of the utility of their approach to build progressively more sophisticated materials.

In this report, we demonstrate a strategy for the incorporation of alkene functional groups into the pore interior, as versatile latent reactive sights amenable to a variety of subsequent transformations.[21] The strategy entails the selective degradation of PLA from core−shell cylinder forming poly(styrene-*b*-isoprene-*b*-lactide) (PS−PI−PLA) triblock copolymers,[25] in conditions that are unreactive toward the main chain and pendant alkene groups populating the exposed polyisoprene chains. By comparing series of PS−PI−PLA triblock copolymers of nearly identical composition yet differing in overall molecular weight, we found a strong apparent influence of molecular size on the ordering and alignment of the terpolymer precursor as well as the integrity of the nanoporous PS−PI framework under various degradation conditions. Finally, we demonstrate the potential versatility of these nanoporous scaffolds through a controlled epoxidation of the alkene functional groups. This overall general strategy is illustrated pictorially in Figure 1.

In the following account we first discuss the synthesis and characterization of multiple PS−PI−PLA triblock copolymers used to probe the breadth of the core−shell cylinder phase boundaries for these materials and then continue with a discussion of the macroscopic alignment and selective degradation of a selected subset of these samples chosen to illustrate the influence of molecular weight. Finally, we discuss the protocols developed for the controlled epoxidation of the pore space.

Results and Discussion

Polymer Synthesis. The synthesis of the PS−PI−PLA precursors was accomplished in two steps using a combination of anionic and controlled ring-opening polymerization techniques. Using a previously reported procedure,[22] hydroxyl-terminated PS−PI diblock copolymer "parent" molecules of different molecular weights were synthesized anionically via sequential styrene and isoprene monomer addition, followed by the addition of a single ethylene oxide unit from which a terminal hydroxyl group was derived.[22b] Living polystyryllithium chains were removed from the reaction mixture just prior to isoprene addition, terminated, and analyzed by size exclusion chromatography (SEC) using PS standards. The molecular weight of the PS fragment was used in combination with the relative PS and PI composition data provided by ^{1}H NMR spectroscopy to extrapolate the overall molecular weight of the PS−PI−OH diblock copolymer. Comparison of the ^{1}H NMR resonances of the methylene protons adjacent to the terminal hydroxyl and the methyl protons of the *sec*-butyl initiator fragment showed hydroxyl end-capping efficiencies between 96% and 99% for all PS−PI diblock copolymers. SEC of the diblock copolymer intermediate revealed a low molecular weight shoulder consistent with a small amount of homopolymer PS, likely terminated during the isoprene crossover step. Example ^{1}H NMR and SEC data (generated from sample **C-0**, Table 1) are given in Figure

Table 1. Molecular and Structural Characteristics of PS−PI−OH and PS−PI−PLA Triblock Copolymers

BCP	$M_{n,PS}$[a]	$M_{n,PI}$[b]	$M_{n,PLA}$[b]	$M_{n,total}$[b]	M_w/M_n[a]	f_{PS}[c]	f_{PI}[c]	f_{PLA}[c]	morphology[d]	$T_{g,PS}$[e]	$T_{g,PI}$[e]
A-0	8.7	3.2		11.9	1.03	0.70	0.30		dis	57.4	−56.3
A-1			3.5	15.4	1.08	0.57	0.24	0.19	hex		
A-2			4.2	16.1	1.07	0.55	0.23	0.22	hex		
A-3			4.5	16.4	1.08	0.54	0.23	0.23	hex		
A-4			5.6	17.5	1.08	0.51	0.22	0.28	hex		
A-5			7.2	19.1	1.09	0.47	0.20	0.33	hex		
A-6			9.0	20.8	1.12	0.44	0.19	0.38	lam		
A-7			9.6	21.5	1.12	0.42	0.18	0.40	lam		
A-8			11.1	23.0	1.17	0.40	0.17	0.43	lam		
B-0	12.3	4.5		16.8	1.03	0.70	0.30		dis	64.3	−60.7
B-1			5.4	22.1	1.07	0.56	0.24	0.20	hex		
B-2			6.2	23.0	1.07	0.54	0.23	0.23	hex		
B-3			8.3	25.1	1.08	0.50	0.21	0.28	hex		
C-0	13.7	5.0		18.7	1.03	0.70	0.30		dis	69.4	−59.9
C-1			5.7	24.4	1.06	0.56	0.24	0.20	hex		
C-2			6.5	25.2	1.07	0.55	0.23	0.22	hex		
C-3			8.9	27.6	1.09	0.51	0.22	0.28	hex		
D-0	23.5	8.5		32.0	1.03	0.70	0.30		hex	92.0	−66.0
D-1			10.7	42.7	1.08	0.55	0.23	0.21	hex		
D-2			14.8	46.8	1.10	0.51	0.22	0.27	hex		
D-3			19.0	51.0	1.13	0.48	0.20	0.32	hex		
D-4			24.4	56.4	1.18	0.44	0.18	0.38	und		

[a] Determined by SEC relative to PS standards (in kg mol^{-1}). [b] Calculated from $M_{n,PS}$ and relative ^{1}H NMR peak intensities (in kg mol^{-1}). [c] Calculated based on nominal densities at 140 °C (ρ_{PS} = 0.969 g cm^{-3}, ρ_{PI} = 0.830 g cm^{-3}, ρ_{PLA} = 1.154 g cm^{-3}). [d] As indentified by SAXS at 25 °C after annealing at 160 °C: dis = disordered, hex = hexagonally packed cylinders, lam = lamellae, and und = undetermined. [e] Determined via DSC heating at 10 °C min^{-1} (in °C).

5a, which are representative of that obtained from the four parent diblock copolymers synthesized.

Subsequent aluminum catalyzed ring-opening polymerization of DL-lactide from the terminal hydroxyl of these parent molecules[9,23−25] produced the final collection of PS−PI−PLA triblock copolymers. As a result of the strong overlap of the ^{1}H NMR resonances associated with the methine proton (4.98−5.28 ppm) of PLA and the vinyl proton of the 4,1 units of polyisoprene (4.90−5.30 ppm), the relative compositions of PLA and PI in the final PS−PI−PLA triblock copolymer were calculated indirectly. By normalizing the peak area in this region to the aromatic proton signal of the polystyrene (6.20−7.26 ppm) fragment, and comparing the value directly with that of the corresponding parent PS−PI−OH diblock, the relative composition of PLA could be extracted. In addition to the residual homopolymer PS shoulder associated with the original diblock copolymer synthesis, SEC of the final triblock copolymers revealed only a small tailing region, consistent with the 1−4% residual unfunctionalized PS−PI diblock copolymer anticipated from the ^{1}H NMR analysis of the hydroxyl end-capping efficiency. Example ^{1}H NMR and SEC data (generated from sample **C-3**) are given in Figure 5b, which are representative of that obtained from the set triblock terpolymers described in this work.

In all, 18 PS−PI−PLA triblock terpolymers were synthesized from four parent hydroxyl-terminated PS−PI diblock copolymers (**A-0**, **B-0**, **C-0**, and **D-0** in Table 1) of identical composition (set at 70:30 (PS:PI) by volume,[26] discussed below) but varied molecular weights. A detailed summary of the molecular and structural characteristics of these 18 polymers is presented in Table 1. Polydispersity indices for all triblock copolymers ranged from 1.07 to 1.18, dependent largely on the reaction conditions adopted for the lactide polymerization step. Lactide polymerizations allowed to proceed to high conversions were susceptible to molecular weight broadening as a result of competing depolymerization which becomes more prevalent as the reaction approaches its equilibrium monomer concentration.[24]

Melt State Phase Behavior. Given the complex phase behavior expressed by ABC triblock copolymer systems,[27] our first priority was to identify a PS-rich region within the PS−PI−PLA compositional phase space occupied by the core−shell cylindrical phase. Relying on a combination of previous reports identifying core−shell cylinder phases in analogous ABC systems[1,17,18,22,25,28−31] and our own experience with similar materials, we synthetically targeted compositions in the lower left corner of the ternary phase diagram, as shown in Figure 2a. We concentrated on the formation of several series (four total) of PS−PI−PLA triblock copolymers, each derived from a single parent PS−PI−OH diblock copolymer. By maintaining the relative ratio of PS to PI at 70:30 by volume[26] in each parent molecule, the resulting series all fall along the same compositional isopleth delineated within the phase triangle in Figure 2a. By adopting this strategy, we were able to easily compare the effects of molecular weight on the processing and degradation behavior of these precursor molecules while limiting the compositional variation between samples.

Identification of the morphologies formed by the block copolymers in Table 1 was based on a combination of direct imaging via transmission electron microscopy (TEM) and structure analysis via small-angle X-ray scattering (SAXS). X-ray diffraction patterns were collected both at 160 °C (in the melt state) and at 20 °C (as a vitrified solid). For each of the samples in Table 1, no transition in morphology was detected as a result of cooling from 160 °C to room temperature. The molecular weight dependence of the sample scattering patterns (20 °C) at two selected compositions ($f_{PLA} = 0.28$ at 17.5 (**A-4**), 27.6 (**C-3**), and 46.8 kg mol^{-1} (**D-2**); $f_{PLA} = 0.38$ at 20.8 (**A-6**) and 56.4 kg mol^{-1} (**D-4**)) is given in Figure 2c,d for a selection of polymer samples. With the exception of copolymers belonging to the highest molecular weight series (series **D**), samples were pressed directly from powders at 160 °C for 10 min and then allowed to cool to room temperature. SAXS data were then collected by first heating the samples back to 160 °C under a vacuum or helium atmosphere for an additional 10 min annealing period and then cooling slowly (∼10 °C min^{-1}) to room temperature where the diffraction patterns were collected. Interestingly, the highest molecular weight series showed considerable kinetic resistance to ordering as determined by SAXS, and developed scattering profiles could only be obtained after channel die processing at 160 °C (see below) followed by an overnight anneal under vacuum at the same temperature. Because these samples were cooled slowly (∼1 °C min^{-1}) back to room temperature following the annealing period, scattering data were collected directly without further thermal treatment.

By comparing the ratio of the higher order scattering vectors ($q = 4\pi/\lambda \sin(\theta/2)$) to the principal scattering vector in each case, assignments of the hexagonally packed cylinder (1: $\sqrt{3}$: $\sqrt{4}$:$\sqrt{7}$:$\sqrt{9}$, etc.) and lamellae (1:$\sqrt{4}$:$\sqrt{9}$:$\sqrt{16}$:$\sqrt{25}$, etc.) phases could be made for most of the triblock copolymer samples in this region (Table 1). Sample **D-4** stands as an exception in this case, for which the peak ratios could not be assigned to any traditional block copolymer morphology on the basis of currently documented bcc, hexagonal, lamellar, gyroid (*Ia*3*d* or $I_1$32), or orthorhombic network (*Fddd*) symmetries. No further attempts at the identification of this material were made. Of note is the considerable decrease in peak sharpness as the molecular weights of the triblock copolymers increase. This was a general trend we again associate with a kinetic resistance to ordering quite often observed in higher molecular weight ABC systems.[32]

TEM was used to confirm the core−shell geometry of the cylindrical domains for those exhibiting the targeted hexagonal symmetry, an example image of which is given in Figure 3 (sample **B-2**). PI domains were stained with OsO_4 vapor prior to imaging to generate the necessary contrast with the adjacent PS and PLA domains. In Figure 3, the PI domains appear as dark shells circumscribing unstained PLA cores, while also surrounded by an unstained PS matrix. On the basis of the hexagonal symmetry confirmed from SAXS data taken on bulk samples, the skewed appearance of the hexagonal packing is likely a simple artifact of the sample orientation relative to the microtome knife during preparation or to the electron beam during imaging. Figure 2b shows the distribution of the core−shell cylinder and lamellae phases as a function of the PLA composition and the overall triblock copolymer molecular weight. Notably, three of the four PS−PI−OH parent molecules appeared by SAXS to be disordered at room temperature, with the highest molecular weight sample **D-0** exhibiting the traditional two-domain hexagonally packed cylinder phase with an order−disorder transition near 190 °C (confirmed by melt-state rheology). This plot also reveals that the window in which the hexagonally packed cylindrical phase forms, spanning PLA volume fractions between 0.19 and 0.33, is quite large and therefore synthetically very accessible. Interestingly, the transition to the lamellar phase in the lower molecular weight samples occurs at the point where the distribution of volume between the PS and PLA end blocks becomes roughly equivalent. For example, we see the first instance of a lamellar morphology in

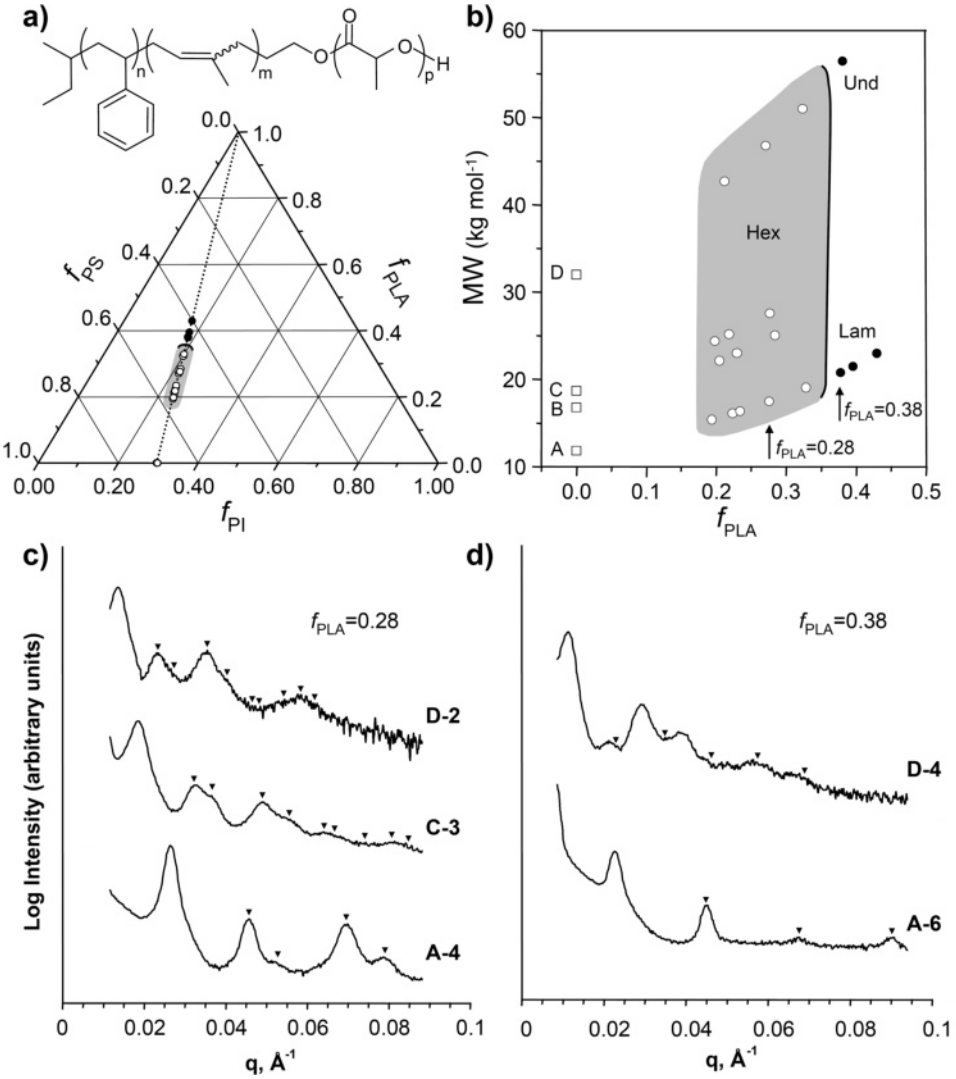

Figure 2. (a**)** Chemical structure of the 18 PS−PI−PLA triblock copolymers reported in Table 1. Volume ratio of PS:PI was held at 70:30 such that all polymers synthesized fell on the same compositional isopleth (dotted line). (b**)** Morphologies determined by SAXS as a function of PLA volume fraction (f_{PLA}) and overall molecular weight for the four triblock copolymer series (A−D) investigated. All boundaries are arbitrarily placed as approximate guides. (c**)** 1D-SAXS profiles showing the hexagonal symmetry (arrows indicate q/q^* ratios of $\sqrt{3}$:$\sqrt{4}$:$\sqrt{7}$:$\sqrt{9}$, etc.) of three samples of identical composition ($f_{PLA} = 0.28$) but increasing molecular weight. (d**)** 1D-SAXS profiles of two additional samples of greater PLA content ($f_{PLA} = 0.38$) demonstrating the transition to a layered (lamellar) symmetry (arrows indicate q/q^* ratios of $\sqrt{4}$:$\sqrt{9}$:$\sqrt{16}$:$\sqrt{25}$, etc.) at lower molecular weights and to an unidentified symmetry at higher molecular weights (peak positions expected for a layered stacking are included for reference).

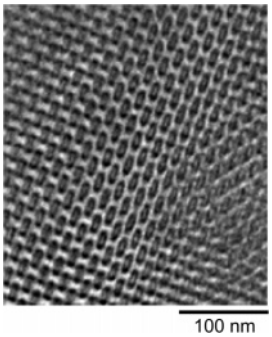

Figure 3. Representative transmission electron micrograph of sample **B-2**, showing the core−shell geometry of the hexagonally packed cylinders. Selectively stained PI domains (OsO_4) form cylindrical shell layers surrounding PLA cores, hexagonally packed in a PS matrix.

sample **A-6** at $f_{PLA} \sim 0.38$ (exact equivalency occurs at $f_{PS} = f_{PLA} \sim 0.41$).

Processing and Alignment. Samples of PS−PI−PLA triblock terpolymer precursors were pressed from a powder into rectangular molds at 160 °C until all bubbles were visibly absent. These prepressed rectangular samples (300−500 mg) were then processed in a home-built channel die[9,19] at 160 °C to form a single elongated rectangular solid (typically $2 \times 2 \times 100$ mm^3), from which macroscopically aligned monolithic pieces (typically $2 \times 2 \times 5$ mm^3) were cut. 2D-SAXS data were then collected on these samples to verify the identity of the morphology after processing and determine the degree of cylindrical domain alignment in a singular direction. As shown in Figure 4a, an aligned sample positioned with the cylindrical axis perpendicular to the incident radiation gives rise to Bragg scattering in which the intensity of the principal wave vector **q*** is highly focused in two spots opposed by 180°. Quantification of the alignment can be made from such 2D scattering data by calculating an associated value of F_2, the second-order orientation factor, which is derived from the normalized orientation distribution function $P(\phi)$ as follows[33]

$$P(\phi) = \frac{I(q^*,\phi)q^{*2}}{\int_0^{\pi} I(q^*,\phi)q^{*2} \sin\phi \, d\phi}$$

where ϕ is the azimuthal angle as defined in Figure 4a and

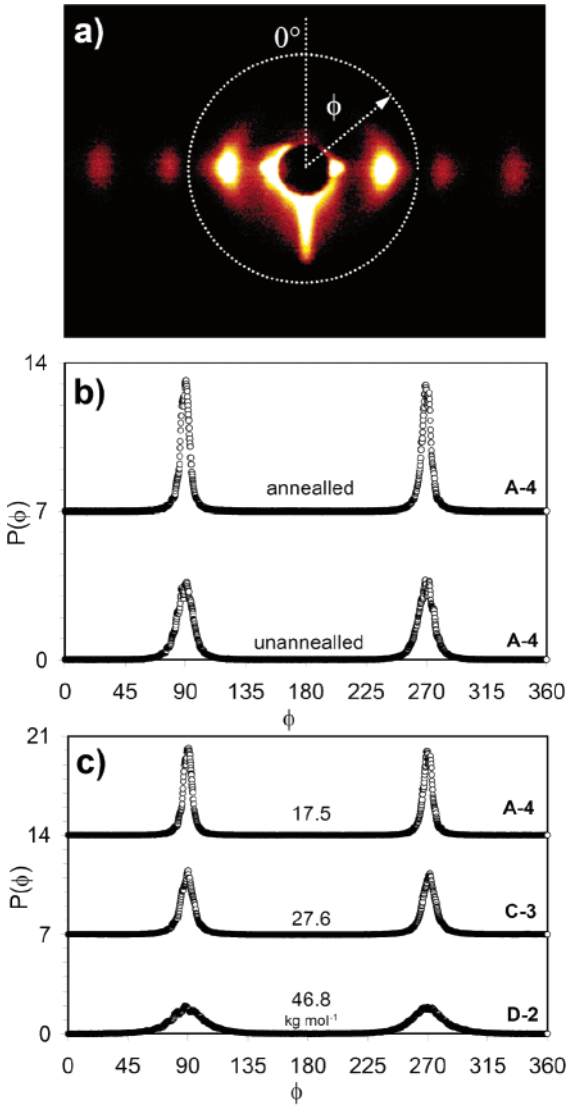

Figure 4. (a) 2D-SAXS scattering pattern for an aligned and postannealed (see below) monolith of sample C-3 ($F_2 = 0.91$). (b) Comparison of the normalized orientation distribution functions, $P(\phi)$, for an aligned monolith of sample **A-4** before ($F_2 = 0.91$) and after ($F_2 = 0.95$) a 16 h postanneal in vacuo at 160 °C. (c) Comparison of the normalized orientation distribution functions, $P(\phi)$, for three aligned and postannealed monoliths of identical compositions ($f_{PLA} = 0.28$) but different molecular weights: **A-4**, 17.5 kg mol^{-1}, $F_2 = 0.95$; **C-3**, 27.6 kg mol^{-1}, $F_2 = 0.91$; **D-2**, 46.8 kg mol^{-1}, $F_2 = 0.78$.

$I(q^*,\phi)$ is the position-dependent scattering intensity at q^*. The $P(\phi)$-weighted average of $\cos^2\phi$ is then obtained

$$\langle \cos^2\phi \rangle = \int_0^{\pi} \cos^2\phi \, P(\phi) \sin\phi \, d\phi$$

from which F_2 can be calculated directly.

$$F_2 = 1 - 3\langle \cos^2\phi \rangle$$

Values of F_2 near one are indicative of a highly aligned sample, with a value equal to one indicating perfect alignment. In our previous work with PLA−PDMA−PS triblock copolymers, we noted that additional thermal annealing of channel die processed samples significantly improved the degree of alignment in the monoliths.[18] We observed similar behavior in the PS−PI−PLA samples investigated in this report, which is captured in Figure 4b by the dramatic narrowing of the normalized orientation distribution function, $P(\phi)$, of a channel die processed sample of **A-4** following a 16 h postanneal at 160 °C in vacuo. The magnitude of the narrowing observed in Figure 4b corresponds to an increase in the calculated F_2 value from 0.91 to 0.95. In general, an increase between 0.03 and 0.07 in the value of F_2 could be achieved for most cylinder-forming samples through postannealing in the melt state. As such, postannealing (160 °C in vacuo) was implemented as a standard processing step prior to any degradation studies.

While improved alignment could be achieved in virtually all samples through a simple postannealing process, the actual degree to which a sample was susceptible to alignment by channel die processing was extremely dependent on the overall molecular weight of the sample itself. Figure 4c shows an overlay of $P(\phi)$ for three samples that have each been channel die aligned and subsequently postannealed at 160 °C in vacuo for 16 h. Notably, these samples share identical compositions and so are varied only in their overall molecular weight ($f_{PLA} = 0.28$ at 17.5 (**A-4**), 27.6 (**C-3**), and 46.8 kg mol^{-1} (**D-2**)). As is clear from the plot, the dramatic drop in the attainable F_2 value with increasing molecular weight demonstrates a very real disparity in the responsiveness of these compositionally identical molecules to the extensional shear fields developed within the channel die.

Selective Chemical Degradation of PLA. For a majority of the PLA-containing block copolymer systems we have used as precursors to nanoporous materials in the past 5 years, we have been able to hydrolytically degrade the polyester block by simply soaking the aligned monoliths in a basic (0.5 N NaOH) solution of 60:40 water:methanol at 65 °C for 7−10 days. This methodology has previously proven to be extremely robust, with aqueous methanol solution serving as an excellent solvent for both the base and the byproducts formed during the course of the degradation, while generally showing no effect on the integrity of the supporting polymer matrix (typically PS). Unfortunately, this methodology proved immediately ineffective for the degradation of PLA from the PS−PI−PLA triblock copolymers described in this report, with less than 2% of the PLA being removed after 14 days under the standard degradation conditions. Notably, these were the first samples investigated in our group in which the PLA core was immediately circumscribed by a shell of PI, a hydrophobic polymer. We believe the hydrophobicity of the PI shell combined with the inherent chain mobility of this domain at the degradation conditions was responsible for effectively screening the PLA core from the surrounding basic solution.

In an effort to find an alternate degradation solution capable of PLA removal from these materials, we performed a small-scale combinatorial screening exercise involving several bases (aqueous NaOH, tetrabutylammonium fluoride (TBAF), sodium methoxide) in combination with a collection of organic additives (methanol, ethanol, 1-propanol, 2-propanol, 1-butanol, *tert*-butyl alcohol, sodium dodecyl sulfate (SDS)) at various concentrations. Temperatures from room temperature to 65 °C, and durations from 1 to 4 weeks, were also screened for most samples. To ensure a consistent testing platform was being used, all screening exercises were performed on monoliths formed from a single triblock copolymer sample (**C-3**). With the exception of methanol, *tert*-butyl alcohol, and 0.5 N NaOH, all other alcohol additives or bases listed above resulted in extreme plasticization of the PS matrix, accompanied by considerable deformation of monolithic forms. Despite the limited influence on the nanoporous framework, the inclusion of neither methanol (standard treatment discussed previously) nor *tert*-butyl alcohol

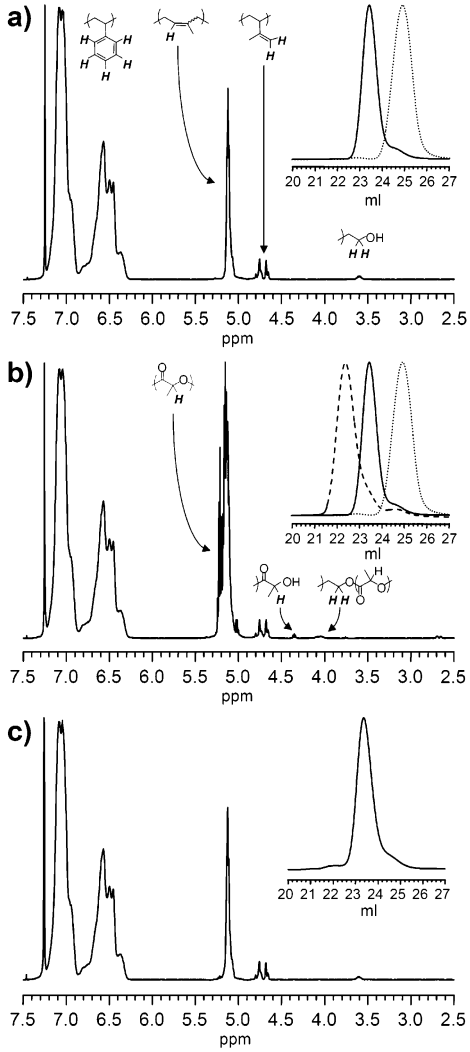

Figure 5. ^{1}H NMR and SEC data for **(a) C-0**, the **C** series PS−PI parent diblock copolymer and associated PS fragment (SEC only), **(b) C-3**, a PS−PI−PLA triblock copolymer with $f_{PLA} = 0.28$ and associated PS fragment (SEC only), and **(c)** a degraded monolith of sample **C-3** showing the near complete removal of PLA.

as a cosolvent with 0.5 N NaOH resulted in any significant PLA degradation.

In contrast, simple treatment of **C-3** with an aqueous solution of 0.1 wt % sodium dodecyl sulfate (SDS) in 0.5 N NaOH at 50 °C for approximately 7−10 days *was* successful at removing greater than 95% of the PLA, with some samples showing 100% degradation. This is in stark contrast to the samples treated without SDS. Example ^{1}H NMR and SEC data of parent diblock copolymer **C-0** together with undegraded and degraded **C-3** samples are shown in Figure 5a−c. We believe that SDS simply acts as a surfactant that facilitates the wetting of the nanoporous structures during degradation of the PLA. Furthermore, there is no swelling of the matrix during degradation in the presence of SDS, and we feel that this is also an important attribute of the SDS containing solutions (see below). Comparison of parts a and c of Figure 5 reveals that post degradation the ^{1}H NMR and SEC data for the PS−PI in the nanoporous monolith almost perfectly match those of the parent PS−PI diblock copolymer (**C-0**) from which it was originally derived. In some samples, a slight high molecular weight shoulder is consistent with a small percentage of PS−PI−PLA triblock copolymer still present in some of the degraded samples. It is likely these small quantities of PLA-containing triblock are located within isolated defects within these soft materials, as their presence was independent of longer reaction times. Scanning electron microscopy (SEM) of the degraded **C-3** monolith both perpendicular and parallel to the pore alignment direction (Figure 6) visually confirmed the expected nanoporous framework and an alignment consistent with the measured predegradation F_2 value of 0.91. Successfully degraded monoliths were removed from the basic surfactant solution, rinsed, and placed into pure water overnight. The rinse water was then exchanged for pure water, and the monoliths were stored wet until further use. Monoliths to be characterized by SAXS, NMR spectroscopy, SEM, SEC, etc., were removed and dried under vacuum at room temperature for 48 h.

Interestingly, when the degradation of a monolith of **C-3** was performed 15 deg higher at 65 °C, only roughly 50% of the PLA was degraded after 10 days. SEM revealed partial collapse of the nanoporous framework with sections of apparent pore coalescence, and ^{1}H NMR spectroscopy and SEC together revealed confirmation of both residual PS−PI−PLA triblock copolymer and low molecular weight PLA within the sample. Thermal analysis of the corresponding PS−PI parent diblock copolymer (**C-0**, Table 1) revealed an upper glass transition temperature of only 69 °C, markedly lower than the expected bulk PS glass transition (∼100 °C). This reduced value is expected given the very weak degree of segregation associated with the disordered state of the block copolymer. Note that the parent diblock copolymers for the two lowest molecular weight series (**A-0** and **B-0**) also show reduced glass transition temperatures for the PS-rich domains. It is likely that the proximity of the matrix glass transition to the degradation temperature (65 °C) was sufficient to induce the partial collapse of the nanoporous framework revealed in the SEM images.[9]

Despite the repeatability of the PLA degradation at 50 °C for samples in the C series (**C-1**, **C-3**), attempts to degrade PLA from aligned monoliths derived from samples in the A and D series (**A-4**, $F_2 = 0.95$; **D-2**, $F_2 = 0.78$) remained problematic, with neither showing any significant (>2%) degradation in the SDS base solution after 14 days. Because of the disparity in the overall molecular weight of these two samples, we feel the cause for their limited degradability is likely of two different sources. Thermal analysis of **A-0**, the corresponding parent diblock copolymer from which **A-4** was derived, revealed an upper glass transition temperature (57.4 °C) very close to the degradation temperature used (50 °C). In an attempt to remove the possibility that degradation was being prohibited by pore collapse or surface rearrangement in solution, degradation at both room temperature and 40 °C was also attempted on aligned monoliths of **A-4**. In neither case was any significant degradation observed, even after 3 weeks at those conditions. It is entirely possible that at such low molecular weights the PS pore wall thickness is insufficient to retain the porous structure upon degradation, and nanoporous materials from such low molecular weight samples cannot easily be fabricated by these methods.[10,34]

The apparent resistance to degradation of the higher molecular weight samples of **D-2** is more difficult to rationalize. Unlike the lower molecular weight samples, the glass transition of the PS domains in the parent diblock copolymer, **D-0** (92 °C, Table 1), was significantly higher than the degradation temperature of 65 °C. As shown in Figures 2c and 4c, both the apparent order and degree of alignment ($F_2 = 0.78$) in these high molecular weight samples are significantly reduced relative to that found in the lower molecular weight samples at similar compositions. It is possible that the marginal level of domain organization is somehow preventing access to the PLA segments defining the core. It should be noted, however, that successful degradation of PLA from PS−PLA diblock copolymer samples with F_2 values in a similar range (0.70−0.80) has been

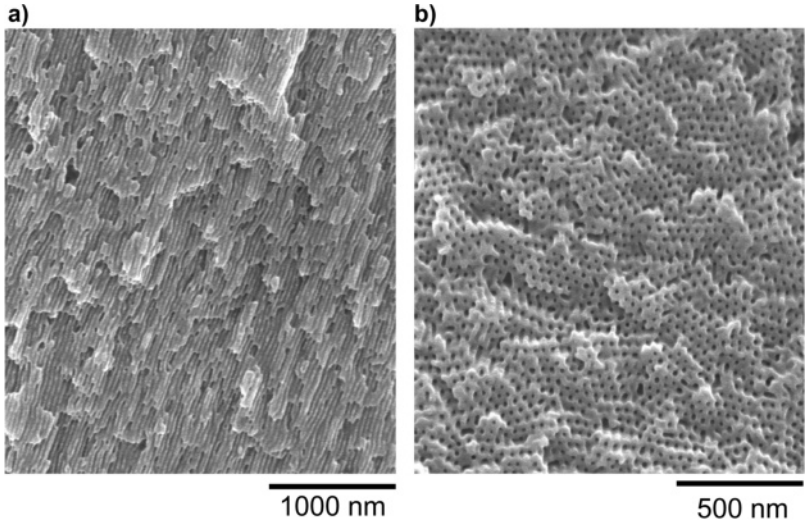

Figure 6. SEM micrographs of a degraded monolith of sample **C-3**, taken **(**a**)** perpendicular and **(**b**)** parallel to the long axis of the pores (F_2 = 0.91 for predegraded monolith).

Table 2. Percent of Alkene Groups Epoxidized as a Function of Time and Reaction Conditions[a]

		% epoxidized as a function of reaction time[e]				
reaction conditions	concentration (M)	1.5 h	4 h	28 h	3 days	5 days
peroxyacetic acid	4.75[b]	8.3[f]				
peroxyacetic acid	0.475[c]	6.1	9.3[f]			
peroxyacetic acid	0.0475[c]	4.2				
MCPBA	0.475[d]	6.5	8.8	25.2	74.4	76.8

[a] All reactions were carried out at room temperature on degraded monoliths of sample **C-3**. [b] Neat solution as purchased, containing 40−45% acetic acid, balance water and hydrogen peroxide (<6%). [c] Aqueous dilution of neat solution. Molarities calculated assuming volume additivity and a neat solution density of 1.13 g cm^{-3}. [d] In *tert*-butyl alcohol. Some water present as contaminant in MCPBA. [e] Measured from point of submersion in reaction solution. All degraded monoliths were roughly 2 × 2 × 4 mm^3. Percent epoxidation determined by ^{1}H NMR spectroscopy. [f] Longer reaction times not investigated due to presence of significant reaction byproducts (^{1}H NMR spectroscopy).

accomplished quite easily.[19] Regardless, it is likely that the nature of the PLA degradation in this system, even at the intermediate molecular weight range, is directly correlated to the presence of the hydrophobic PI block in the domain surrounding the PLA core.

Controlled Epoxidation of PI. The PI coating on the internal pore surface of the degraded monoliths provides inherently reactive alkene handles through which further chemical modifications can be made. As a demonstration, we explored two primary routes toward the controlled epoxidation of these di- and trisubstituted alkenes following PLA degradation. Epoxide groups represent an ideal target due to their excellent electrophilic character toward addition reactions with many functional groups, including alcohols and amines. Importantly, the inclusion of epoxide groups at any other step in the fabrication process is restricted by their inherent thermal and chemical sensitivity. For example, PS−PI−PLA could be epoxidized with much greater efficiency in solution prior to channel die processing; however, subjecting the epoxide groups to the basic conditions employed in subsequent PLA degradation would undoubtedly precipitate their ring opening to form the corresponding polyol. While this perhaps represents another interesting route to nanoporous PS monoliths with hydrophilic pore character, our efforts here were focused on methods of integrating the epoxide groups as latent coupling agents for the generation of more sophisticated support frameworks.

We employed two peroxide-based strategies for in-situ epoxidation of PI. Table 2 gives the percent of the alkene groups epoxidized as a function of time using either peroxyacetic acid in acetic acid/water solutions or *m*-chloroperoxybenzoic acid (MCPBA) in *tert*-butyl alcohol (*t*-BuOH)/water solutions. The choice of epoxidation conditions were largely based on the solvent compatibility with the nanoporous PS framework, as any slight degree of plasticization is a threat to trigger its collapse. All epoxidation reactions were done on degraded monoliths derived from sample **C-3**. Notably, our preliminary attempts utilizing monoliths dried in vacuo following the degradation rinse step exhibited a strong resistance to rewetting in either of these reaction media; this is presumably due to the strong incompatibility of the reaction solutions with the internal PI coating. To circumvent this issue, degraded monoliths were stored under water following the degradation rinse step, such that the wetting achieved during the degradation process (in the presence of SDS) was maintained. Monoliths used in this way were taken directly from storage under water and placed immediately into their designated reaction solutions after quickly blotting excess water from the external surfaces.

The epoxidation with peroxyacetic acid was initially carried out in a "neat" solution of 32 wt % (4.75 M) peroxyacetic acid in dilute acetic acid. Subsequently, two aqueous dilutions (0.475 and 0.0475 M) were also investigated. All reactions were carried out at room temperature. Perhaps not unsurprisingly, we found these conditions amenable to the subsequent acid catalyzed ring opening of the formed epoxide groups (among other possible side reactions), which competitively limited the overall epoxide conversion possible before significant byproduct formation was detected (^{1}H NMR spectroscopy). We suspect that the byproducts observed likely stemmed from hydrolysis of the epoxide groups under the reaction conditions. In monoliths treated with the highest peroxyacetic acid concentrations, conversion of the alkene groups was rapid, with almost 75% of them converted after only 1.5 h; however, only 8.3% of these original alkene

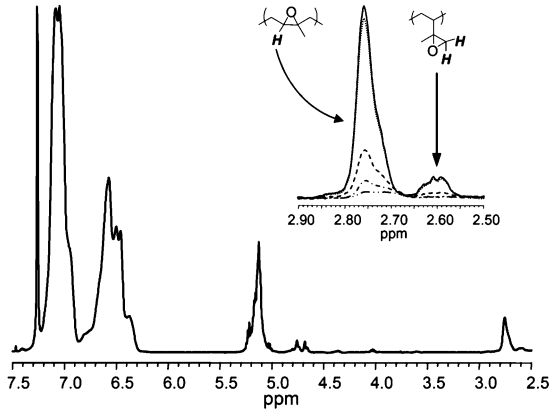

Figure 7. ^{1}H NMR data for a degraded monolith of sample **C-3** that has been 25.2% epoxidized in 0.475 M MCPBA (*t*-BuOH, 28 h). The inset shows the growth of the proton signal associated with the increasing fraction of epoxide groups in the monolith as a function of reaction time in the MCPBA solution. Signals correspond directly to the entries in Table 2, covering 1.5 h (least signal intensity) to 5 days (highest signal intensity). Spectra have been normalized to a constant PS intensity.

groups existed as the desired epoxide. As anticipated, dilution of the peroxyacetic acid solution decreased the rate of overall conversion but did not entirely eliminate the competing formation of the undesirable byproducts. For example, at the intermediate peroxyacetic acid concentration (0.475 M), we estimated that after only 4 h of reaction time nearly 25−30% of the converted alkene groups (13% total) were present in forms other than epoxides.

On the basis of the limited impact of *t*-BuOH on the integrity of the PS matrix we observed during our combinatorial degradation study, we pursued an alternate epoxidation strategy employing MCPBA as the oxidizing agent with *t*-BuOH as the mediating solvent. As above, reactions were carried out at room temperature. Reaction solutions containing MCPBA were made by dissolving 77 wt % MCPBA (Aldrich, balance *m*-chlorobenzoic acid and water) in a volume of *t*-BuOH to produce 0.475 M solutions mirroring the intermediate concentrations used in the peroxyacetic acid reactions described above. Unlike the peroxyacetic acid solutions which contained a large amount of residual acetic acid, residual *m*-chlorobenzoic acid contained in the MCPBA was insoluble in *t*-BuOH and was filtered from the reaction solution using a 0.2 μm filter prior to the addition of the degraded monolith. Under these new reaction conditions, the undesirable hydrolysis of the epoxide groups, as well as any other apparent side reactions, was effectively eliminated, and the epoxidation proceeded smoothly to give ~75% conversion of all alkene groups within 3 days (Table 2). Additional increases in reaction time beyond the 3 day mark showed very little improvement in conversion; we surmise that alkene groups located near the PS−PI interface may have limited accessibility, and conversion of these groups becomes prohibitively slow due to the high density and reduced mobility of the PI brush near this interface. Despite this apparent upper limit in alkene group conversion, the rate control and product purity exhibited by the MCPBA approach render this methodology extendable to other alkene-containing nanoporous materials.

Figure 7 shows the ^{1}H NMR and SEC data of a sample monolith epoxidized to 25.2% (28 h). Comparison with Figure 5c, depicting the ^{1}H NMR and SEC data for the degraded monolith prior to epoxidation, shows the expected decrease in the vinyl proton signals of polyisoprene (4,1 units, 5.04−5.18 ppm; 4,3 units, 4.64−4.84 ppm) and their expected reemergence upfield after conversion to the epoxide (4,1 units, 2.67−2.95 ppm; 4,3 units, 2.55−2.67 ppm). The inset of Figure 7 shows the growth of the proton signal associated with the increasing fraction of epoxide groups in the monolith as a function of reaction time. Figure 8 depicts an SEM image of a sample of degraded **C-3** treated with 0.475 M MCPBA in *t*-BuOH for 5 days. Despite treatment for such an extended duration, the image clearly shows retainment of the nanoporous structure at 77% epoxidation, although the high degree of alignment observed prior to epoxidation seems to be diminished. Calculation of F_2 values for samples with similar degrees of epoxidation gave values ranging from 0.68 to 0.72, consistent with the moderate loss of alignment apparent in the SEM image of Figure 8. It is notable that upon epoxidation to such high conversions the nanoporous monolith becomes surprisingly brittle. Future improvements in the robustness of the PS matrix through such means as chemical cross-linking, for example, may help provide both improved mechanical integrity and improved retention of alignment under mild solvent conditions such as those used in the epoxidation reactions above.

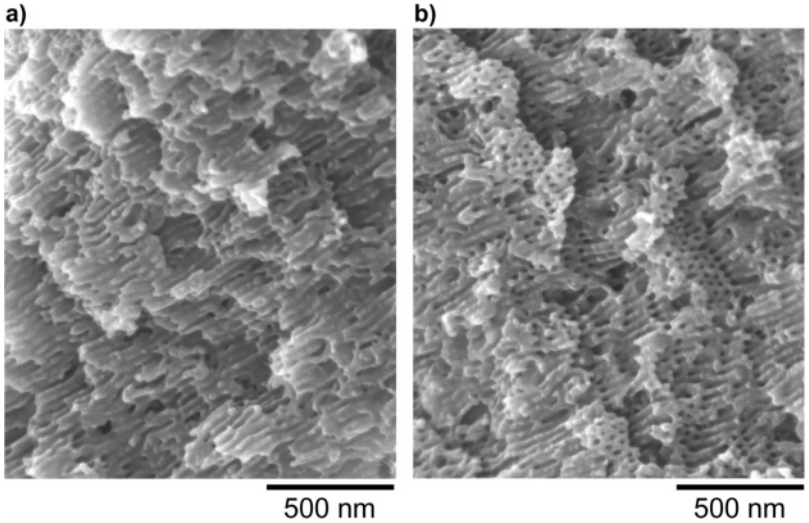

Figure 8. SEM micrographs of a 77% epoxidized sample of nanoporous **C-3**, taken after 5 days in 0.475 M MCPBA in *t*-BuOH. Images are taken roughly (a**)** perpendicular and **(**b**)** at 45° to the long axis of the pores. Nanoporous structure persists through the epoxidation; however, some loss of pore alignment may be occurring.

Conclusions

Exploiting the core−shell cylinder morphology formed in PS−PI−PLA triblock copolymers as a template, we produced nanoporous PS monoliths with PI-coated pores. The degree of order and alignment achievable in the PS−PI−PLA systems was found to be a strong function of molecular weight for a given triblock copolymer composition, with higher molecular weight samples being far less responsive to channel die alignment. The presence of the hydropohobic PI block in the domain circumscribing the PLA core seemed to have a significant influence on the PLA degradation process, as our standard degradation conditions (0.5 N NaOH in 60:40 water:methanol at 65 °C) were ineffective. We identified a 0.1 wt % solution of SDS in 0.5 N NaOH as a suitable degradation agent capable of efficiently removing >95% of the PLA. Degradability, however, was limited to samples with intermediate overall molecular weights (25−28 kg mol^{-1}), as low (18 kg mol^{-1}) and high (47 kg mol^{-1}) molecular weight samples of identical composition showed resistance to degradation. Subsequent epoxidation of the alkene units in the PI coating was approached by two oxidative methods: one based on peroxyacetic acid in acetic acid/water and the other on MCPBA in *t*-BuOH/water. The latter method proved superior, eliminating the side reactions prevalent using peroxyacetic acid and permitting controlled epoxidations up to 75−80%. SEM was able to verify the retainment of the nanoporous structure following epoxidation; however, some loss of pore alignment was apparent, with F_2 values dropping from the 0.87−0.91 range to the 0.68−0.72 range. Despite this marginal loss in alignment, our ability to successfully epoxidize the alkene groups in these PI surface-coated PS monoliths suggests such nanoporous materials may prove excellent building blocks from which more complex nanoporous materials can be fabricated.

Experimental Section

Materials. Styrene (99%, 10−15 ppm 4-*tert*-butylcatechol inhibitor, Aldrich) and ethylene oxide (99.5+%, compressed gas, Aldrich) were purified by successive distillations from dibutylmagnesium (0.1 mmol/g styrene, 1.0 M solution in heptane, Aldrich) under a static vacuum of 10−20 mTorr. Isoprene (99%, 100 ppm *p*-*tert*-butylcatechol inhibitor, Aldrich) was purified by successive distillations from *n*-butyllithium (0.25 mmol/g isoprene, 2.5 M solution in hexanes, Aldrich). Cyclohexane and toluene (HPLC grade) were purified by passage through activated alumina (A-2 (12 × 32), LaRoche) and supported copper redox catalyst (CU-0226S (previously Q-5 reactant), Engelhard) under high-purity argon in home-built columns, as described by Pangborn et al.[35] *sec*-Butyllithium (1.3 M solution in cyclohexane, Aldrich) was used as received. The concentration was determined prior to use using the Gilman double titration method[36] with 1,2-dibromoethane (99%, Aldrich). DL-Lactide was purified by recrystallization from ethyl acetate and stored under dry nitrogen in a glovebox. High-purity argon (99.998%, Air Products) was passed through an OMI-2 Nanochem resin purification column (Air Products) to remove excess oxygen and moisture. Peroxyacetic acid (32 wt %, Aldrich), MCPBA (77 wt %, Aldrich), and all other common chemicals were used as received without further purification.

Synthesis of PS−PI−OH (Example Amounts and Conditions Given for Sample C-0). The synthesis of PS−PI−OH diblock copolymers was carried out using the previously reported procedures of Bailey et al.[22] This general approach is briefly summarized below for the synthesis of sample **C-0**. Sequential anionic polymerization of styrene (76.84 g, 8 h) and isoprene (28.15 g, 8 h) was initiated with *sec*-butylithium (3.88 mL, 1.45 M by titration[36]) in dry cyclohexane (1 L) at 40 °C under a slight positive pressure of argon. Ethylene oxide was added (9.12 g, 20 h) as an end-capping agent, and the reaction was cooled to room temperature. The terminal oxyanion was quenched with acidic methanol (50 mL, 49:1 MeOH:HCl (conc)), and the product precipitated from 5:1 MeOH:IPA (6 L). Filtration and drying in vacuo (25 °C, 48 h) gave the polymeric alcohol as a coarse white powder. Yield = 103.1 g (98%). SEC (PS standards): PS fragment M_n = 13.7 kg/mol, M_w/M_n = 1.03, PS−PI−OH M_n (by ^{1}H NMR spectroscopy and SEC of PS fragment.) = 18.7 kg mol^{-1}, M_w/M_n = 1.03. ^{1}H NMR (ppm downfield from TMS): 6.20−7.26 (b, −(C$_6$*H*$_5$)), 4.90−5.30 (b, −CH$_2$−C*H*═C(CH$_3$)−CH$_2$−), 4.60−4.90 (b, C*H*$_2$═C(CH$_3$)−), 3.5−3.7 (m, −CH$_2$−OH), 0.84−2.40 (b, CH$_2$═C(C*H*$_3$)−C(R)*H*−C*H*$_2$−, −C*H*$_2$−CH═C(C*H*$_3$)-C*H*$_2$−, and C$_6$H$_5$−C(R)*H*−C*H*$_2$−), 0.5−0.78 (m, −C*H*$_3$, initiator fragment).

Synthesis of PS−PI−PLA (Example Amounts and Conditions Given for Sample C-3). The polymerization PLA from the hydroxylated end of the PS−PI−OH parent molecules was carried out using procedures analogous to those reported by Wang et al. for the polymerization of PLA from hydroxylated polybutadienes.[23] This general approach is briefly summarized below for the synthesis of sample **C-3**. PS−PI−OH diblock copolymer (2.0 g, 0.107 mmol, 18.7 kg mol^{-1}) was combined with dry toluene (10 mL) in a glass pressure vessel inside a nitrogen glovebox, and the contents were vigorously stirred until all polymer was dissolved. Triethylaluminum (54 μL, 1.0 M in heptane, [OH]:[Al] = 2:1) was then added via syringe, the vessel sealed, and allowed to stir in the glovebox overnight at room temperature. DL-Lactide monomer (2 g, 13.9 mmol) was added, and the sealed reaction vessel was removed from the glovebox and placed immediately into an oil bath at 100 °C. After 60 min the vessel was removed and immediately cooled under running water to room temperature, after which aqueous HCl (1.5 M, 1.0 mL) and CH_2Cl_2 (3−5 mL) were added to terminate and dilute the reaction mixture. After 20 min of stirring, the PS−PI−PLA triblock copolymer was precipitated into methanol (350 mL), filtered, and dried in vacuo (25 °C, 48 h) to produce a fine white powder. Yield = 2.95 g (47.5% lactide conversion). M_n (by ^{1}H NMR spectroscopy and SEC of PS fragment) = 27.6 kg mol^{-1}, PDI (PS standards): M_w/M_n = 1.09. ^{1}H NMR (ppm downfield from TMS): 6.20−7.26 (b, −CH(C$_6$*H*$_5$)), 4.90−5.30 (b, −CH$_2$−C*H*═C(CH$_3$)−CH$_2$−), 4.98−5.28 (b, −C(O)C*H*(CH$_3$)O−), 4.60−4.90 (b, C*H*$_2$═C(CH$_3$)−), 4.30−4.42 (m, −C(O)C*H*(CH$_3$)OH), 3.95−4.15 (b, −CH$_2$C*H*$_2$−O−), 2.60−2.75 (bd, −C(O)CH(CH$_3$)O*H*), 0.84−2.40 (b, CH$_2$═C(C*H*$_3$)−C(R)*H*−C*H*$_2$−, −C*H*$_2$−CH═C(C*H*$_3$)-C*H*$_2$−, −C(O)CH(C*H*$_3$)O−, and C$_6$H$_5$−C(R)*H*−C*H*$_2$−), 0.5−0.78 (m, −C*H*$_3$, initiator fragment).

PI Epoxidation in PS−PI Nanoporous Monoliths (Example Amounts and Conditions Given for a Degraded Monolith Derived from Sample C-3). Epoxidation was attempted by two methods. In both cases, degraded monoliths (approximately 2 × 2 × 4 mm^3, 11−12 mg) stored under water (pores completely wetted) were placed directly in the reaction solutions (one monolith per 1 mL of solution) after quickly blotting any excess water from the external surface. Reaction times are all based on the point of submersion. *Method 1*. Degraded monoliths were placed directly into one of three peroxyacetic acid (32 wt %, Aldrich, 40−45% acetic acid, balance water and hydrogen peroxide (<6%)) solutions: 4.75, 0.475, and 0.0475 M. The highest concentration represents that of the neat peroxyacetic acid reagent, as purchased, with all dilutions done with DI water only. The ratio of [alkene]:[peroxide], given a 1 mL reaction volume and 12 mg monolith, corresponds to approximately 100, 10, and 1 time(s) excess, respectively. At the end of the specified reaction times (see Results and Discussion for times used), monoliths were removed from reaction solutions, rinsed, and placed in DI water (20 mL) overnight. Monoliths were then removed from the rinse solution and dried in vacuo (25 °C, 48 h) for further analysis. ^{1}H NMR spectroscopy revealed significant byproducts at early reaction times, and this method was abandoned in favor of *method 2*. Degraded monoliths were placed directly into a 0.475 M solution of MCPBA in *t*-BuOH/water prepared as follows. MCPBA (77 wt %, Aldrich, balance *m*-chlorobenzoic acid and water) was dissolved in *t*-BuOH, and the remaining solid (*m*-chlorobenzoic acid) was filtered from the solution by syringe using a 0.2 μm filter. The ratio of [alkene]:

[peroxide], given a 1 mL reaction volume and 12 mg monolith, corresponds to approximately 10 times excess. At the end of the specified reaction times, the monoliths were removed from the reaction solutions, rinsed, and placed in DI water (20 mL) overnight. Monoliths were then removed from the rinse solution and dried in vacuo (25 °C, 48 h) for further analysis. ^{1}H NMR (ppm downfield from TMS): 6.20−7.26 (b, −(C$_6$*H*$_5$)), 4.90−5.30 (b, −CH$_2$−C*H*═C(CH$_3$)−CH$_2$−), 4.60−4.90 (b, C*H*$_2$═C(CH$_3$)−), 3.5−3.7 (m, −CH$_2$−OH), 2.67−2.95 (b, −CH$_2$−C*H*(O)C(CH$_3$)−CH$_2$−, epoxidized 4,1-units), 2.55−2.67 (b, C*H*$_2$(O)C(CH$_3$)−, epoxidized 4,3-units), 0.84−2.40 (b, CH$_2$═C(C*H*$_3$)−C(R)*H*−C*H*$_2$−, −C*H*$_2$−CH═C(C*H*$_3$)−C*H*$_2$−, and C$_6$H$_5$−C(R)*H*−C*H*$_2$−), 0.5−0.78 (m, −C*H*$_3$, initiator fragment).

Measurements. SEC data were obtained using tetrahydrofuran (35 °C, 1 mL/min) as the mobile phase on an HP 1100 series liquid chromatography system equipped with Jordi divinylbenzene columns (10^5, 10^3, and 500 Å) and an HP 1047A RI detector. All ^{1}H NMR data were taken at room temperature in $CDCl_3$ on a Varian VI-500 spectrometer. SAXS experiments were run on a home-built beamline at the University of Minnesota, using Cu Kα radiation ($\lambda = 1.54$ Å) generated on a Rigaku rotating anode. 2D data were collected on a Bruker Hi-Star area detector. SEM analysis was performed on a Hitachi S-900 FE-SEM. Fractured monoliths were coated with a 2 nm thick Pt layer via direct Pt sputtering prior to imaging. TEM analysis was performed on a JEOL 1210 transmission electron microscope operating at 120 kV. Samples were cryomicrotomed at −40 to −60 °C and stained with OsO_4 vapor for ∼7 min. DSC analysis was performed on a TA Instruments Q1000 at 10 °C/min. Glass transition temperatures were recorded on a second heating run after samples were cooled from 150 °C at 10 °C/min.

Acknowledgment. This work was supported by the National Science Foundation (DMR-0094144), by the David and Lucile Packard Foundation, and in part by the MRSEC Program of the National Science Foundation under Award DMR-0212302. We also thank John Zupancich for assistance with the TEM measurements.

References and Notes

(1) Hillmyer, M. A. *Adv. Polym. Sci.* **2005**, *190*, 137−181.
(2) Chan, V. Z. H.; Hoffman, J.; Lee, V. Y.; Iatrou, H.; Avgeropoulos, A.; Hadjichristidis, N.; Miller, R. D.; Thomas, E. L. *Science* **1999**, *286*, 1716−1719.
(3) Hatton, B.; Landskron, K.; Whitnall, W.; Perovic, D.; Ozin, G. A. *Acc. Chem. Res.* **2005**, *38*, 305−312.
(4) Hedrick, J. L.; Miller, R. D.; Hawker, C. J.; Carter, K. R.; Volksen, W.; Yoon, D. Y.; Trollsas, M. *Adv. Mater.* **1998**, *10*, 1049−1053.
(5) Pai, R. A.; Humayun, R.; Schulberg, M. T.; Sengupta, A.; Sun, J. N.; Watkins, J. J. *Science* **2004**, *303*, 507−510.
(6) Raman, N. K.; Anderson, M. T.; Brinker, C. J. *Chem. Mater.* **1996**, *8*, 1682−1701.
(7) Zhao, D. Y.; Feng, J. L.; Huo, Q. S.; Melosh, N.; Fredrickson, G. H.; Chmelka, B. F.; Stucky, G. D. *Science* **1998**, *279*, 548−552.
(8) Soler-Illia, G.; Crepaldi, E. L.; Grosso, D.; Sanchez, C. *Curr. Opin. Colloid Interface Sci.* **2003**, *8*, 109−126.
(9) Zalusky, A. S.; Olayo-Valles, R.; Taylor, C. J.; Hillmyer, M. A. *J. Am. Chem. Soc.* **2001**, *123*, 1519−1520.
(10) Cavicchi, K. A.; Zalusky, A. S.; Hillmyer, M. A.; Lodge, T. P. *Macromol. Rapid Commun.* **2004**, *25*, 704−709.
(11) Wolf, J. H.; Hillmyer, M. A. *Langmuir* **2003**, *19*, 6553−6560.
(12) Mingqi Li, M.; Coejart, C. A.; Ober, C. K. *Adv. Polym. Sci.* **2005**, *190*, 183−226.
(13) (a) Mansky, P.; Harrison, C. K.; Chaikin, P. M.; Register, R. A.; Yao, N. *Appl. Phys. Lett.* **1996**, *68*, 2586−2588. (b) Thurn-Albrecht, T.; Schotter, J.; Kastle, G. A.; Emley, N.; Shibauchi, T.; Krusin-Elbaum, L.; Guarini, K.; Black, C. T.; Tuominen, M. T.; Russell, T. P. *Science* **2000**, *290*, 2126−2129. (c) Thurn-Albrecht, T.; Steiner, R.; DeRouchey, J.; Stafford, C. M.; Huang, E.; Bal, M.; Tuominen, M.; Hawker, C. J.; Russell, T. P. *Adv. Mater.* **2000**, *12*, 787−790.
(14) (a) Olayo-Valles, R.; Lund, M. S.; Leighton, C.; Hillmyer, M. A. *J. Mater. Chem.* **2004**, *14*, 2729−2731. (b) Olayo-Valles, R.; Guo, S.; Lund, M. S.; Leighton, C.; Hillmyer, M. A. *Macromolecules* **2005**, *38*, 10101−10108.
(15) For recent work on the development of ABC triblock thin films for nanolithographic applications see: Bang, J.; Kim, S. H.; Drockenmuller, E.; Misner, M. J.; Russell, T. P.; Hawker, C. J. *J. Am. Chem. Soc.* **2006**, *128*, 7622−7629. Also, an early report describing the etching of ABC triblock terpolymers has been published: Liu, G.; Ding, J.; Stewart, S. *Angew. Chem., Int. Ed.* **1999**, *38*, 835−838.
(16) Mao, H.; Arrechea, P. L.; Bailey, T. S.; Johnson, B. J. S.; Hillmyer, M. A. *Faraday Discuss.* **2005**, *128*, 149−162.
(17) Rzayev, J.; Hillmyer, M. A. *Macromolecules* **2005**, *38*, 3−5.
(18) Rzayev, J.; Hillmyer, M. A. *J. Am. Chem. Soc.* **2005**, *127*, 13373−13379.
(19) Zalusky, A. S.; Olayo-Valles, R.; Wolf, J. H.; Hillmyer, M. A. *J. Am. Chem. Soc.* **2002**, *124*, 12761−12773.
(20) Mao, H.; Hillmyer, M. A. *Soft Matter* **2006**, *2*, 57−59.
(21) McGrath, M. P.; Sall, E. D.; Tremont, S. J. *Chem. Rev.* **1995**, *95*, 381−398.
(22) (a) Bailey, T. S.; Pham, H. D.; Bates, F. S. *Macromolecules* **2001**, *34*, 6994−7008. (b) Quirk, R. P.; Mathers, R. T.; Wesdemiotis, C.; Arnould, M. A. *Macromolecules* **2002**, *35*, 2912−2918.
(23) Wang, Y. B.; Hillmyer, M. A. *Macromolecules* **2000**, *33*, 7395−7403.
(24) Wang, Y.; Hillmyer, M. A. ACS *Div. Polym. Mater. Sci. Eng. Prepr.* **2001**, *84*, 634.
(25) Guo, S.; Rzayev, J.; Bailey, T. S. *Zalusky*, A. S.; Olayo-Valles, R.; Hillmyer, M. A. *Chem. Mater.* **2006**, *18*, 1719−1721.
(26) Volume fractions were calculated from nominal densities at 140 °C ($\rho_{PS} = 0.969$ g cm^{-3}, $\rho_{PI} = 0.830$ g cm^{-3}, $\rho_{PLA} = 1.154$ g cm^{-3}). See: Fetters, L. J.; Lohse, D. J.; Richter, D.; Witten, T. A.; Zirkel, A. *Macromolecules* **1994**, *27*, 4639−47.
(27) Bates, F. S.; Fredrickson, G. H. *Phys. Today* **1999**, *52*, 32−38.
(28) Balsamo, V.; Gyldenfeldt, F. v.; Stadler, R. *Macromolecules* **1999**, *32*, 1226−1232.
(29) Breiner, U.; Krappe, U.; Abetz, V.; Stadler, R. *Macromol. Chem. Phys.* **1997**, *198*, 1051−1083.
(30) Gido, S.; Schwark, D. W.; Thomas, E. L. *Macromolecules* **1993**, *26*, 2636−2640.
(31) Huckstadt, H.; Gopfert, A.; Abetz, V. *Polymer* **2000**, *41*, 9089−9094.
(32) Epps, T. H.; III.; Bates, F. S. *Macromolecules* **2006**, *39*, 2676−2682.
(33) deGennes, P. G.; Prost, J. *The Physics of Liquid Crystals;* Oxford University Press: New York, 1993.
(34) Muralidharan, V.; Hui, C. Y. *Macromol. Rapid Commun.* **2004**, *25*, 1487−1490.
(35) Pangborn, A. B.; Giardello, M. A.; Grubbs, R. H.; Rosen, R. K.; Timmers, F. J. *Organometallics* **1996**, *15*, 1518−20.
(36) Gilman, H.; Cartledge, F. K. *J. Organomet. Chem.* **1964**, *2*, 447−454.

MA061892B